Appl. Phys. B 92, 103–109 (2008)
DOI: 10.1007/s00340-008-3056-9

Applied Physics B
Lasers and Optics

A.A. KOSTEREV[1,✉]
Y.A. BAKHIRKIN[1]
F.K. TITTEL[1]
S. MCWHORTER[2]
B. ASHCRAFT[2]

QEPAS methane sensor performance for humidified gases

[1] Rice University, Electrical and Computer Engineering Department, Houston, TX 77005, USA
[2] Hydrogen Technology Research Laboratory, Savannah River National Laboratory, Aiken, SC 29808, USA

Received: 18 April 2008
Published online: 30 May 2008 •

ABSTRACT A trace gas sensor based on quartz enhanced photoacoustic spectroscopy (QEPAS) was evaluated using humidified nitrogen samples and ambient air. Relaxation processes following vibrational excitation of $2\nu_3$ state of CH_4 were investigated. Sensor performance at different gas pressures could be predicted based on a developed kinetic model. The experimentally determined normalized detection sensitivity for CH_4 in humid gas is 1.0×10^{-8} cm^{-1} W/Hz$^{1/2}$.

PACS 82.80.Kq; 42.62.Fi

1 Introduction

Real-time monitoring of trace gas contaminates is important in the optimization of the industrial processing conditions, for applications in chemical weapons detection, breath analysis, and in automotive and industrial emission monitoring. The quantification of trace gases using quartz enhanced (QE) photoacoustic spectroscopy (PAS) approach [1] is a rapidly developing technique for spectroscopic chemical analysis. Since its appearance in 2002, quartz enhanced photoacoustic spectroscopy (QEPAS) [1, 2] has been used with several laser sources including near-infrared (NIR) and mid-infrared (MIR) semiconductor lasers (both distributed feedback [DFB] and external cavity), optical parametric oscillator (OPO), and fiber amplifiers, and was applied to detection of various chemical species including molecules with unresolved vibrational absorption bands. The essence of QEPAS is in detecting optically generated sound by means of a quartz tuning fork (QTF), an electromechanical oscillator which possesses a set of unique properties such as an extremely high quality (Q) factor, small size, and low sensitivity to background acoustic noise. All QEPAS-based sensors reported to date use commercially mass-produced QTFs (used by the watch and clock industry as a frequency standard) oscillating at 32.8 kHz, which determines the optical excitation modulation frequency. This frequency is considerably higher than what is typically used in conventional photoacoustic spectroscopy (PAS) sensors, and for some molecules (e.g. CO and CO_2) is comparable to or exceeds the vibrational-to-translational (V–T) energy transfer rate in gases. As a result, the observed photoacoustic signal may exhibit reduced amplitude if compared to conventional PAS and a significant phase shift with respect to the optical excitation. At the same time, the phase information can be used to enhance the chemical selectivity and to monitor the presence of other gas mixture constituents such as H_2O vapor [5–7]. Hence, the study of the relevant molecular V–T relaxation process(es) is an essential part of QEPAS implementation and optimization of the sensor performance.

In this work we report the detection and monitoring of trace methane (CH_4) concentrations using a compact QEPAS-based sensor, and we explore the relevant energy transfer processes in CH_4/N_2 and $CH_4/H_2O/N_2$ gas mixtures. The results are compared with the recently published work [8] where a similar laser was used to detect trace methane by means of conventional PAS. The measurement of trace methane content in gas streams is important for technological processes used at the Savannah River National Laboratory site, which was the main motivation to carry out the work reported in this paper. However, methane detection is of considerable interest for a wide range of applications. Methane is a major greenhouse gas; its detection is also important for pinpointing leaks in gas transportation pipelines, and for safety in coal mines.

2 Description of sensor

The architecture of the methane sensor used for this work is identical to the architecture outlined in [1] and later implemented for HCN detection using a fiber coupled NIR diode laser [9]. Briefly, radiation of a fiber-coupled DFB diode laser operating at 1.65 μm was split in a 99/1 power ratio using a fiber beam splitter. This allows 1% of the optical power to be directed to a fiber coupled, sealed reference gas cell (Wavelength References, Mulino, Oregon) equipped with a photodiode (PD), while 99% is directed to the photoacoustic absorption detection module (ADM) consisting of a QTF and an organ pipe type acoustic microresonator (μR). The electrical response of the QTF to the laser induced acoustic wave is detected using a transimpedance amplifier with a $R_{FB} = 10$ MΩ feedback resistor. The diode laser current and temperature are adjusted so that the laser optical frequency is close to 6057.1 cm^{-1}, where four partially merged CH_4 absorption lines are located. A sinusoidal dither was added to the laser current to induce wavelength modulation (WM) at a frequency $f = f_0/2$, where f_0 is the resonant frequency of

✉ Fax: +1-713-348-5686, E-mail: akoster@rice.edu

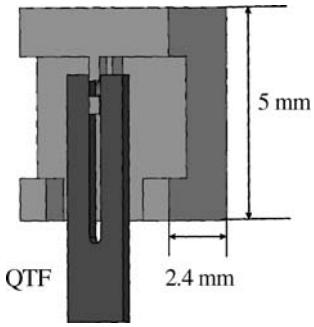

FIGURE 1 Design of the acoustic microresonator used in the present work. The *darker shaded part* is a QTF, and the *lighter part* is one of the two parts constituting the microresonator (μR). The second part (not shown) is a rectangular aluminum block with an identical and collinear ∅0.35 mm channel

the QTF. The QTF signal is detected at $2f = f_0$ frequency. A control electronics unit (CEU) performed all the required functions, such as the control of the diode laser drive current and temperature, wavelength locking, and data acquisition. Wavelength locking function was executed using a $3f$ component of the PD output as an error signal in a feedback loop. The reference cell (with $l = 27$ mm optical pathlength) was filled with a mixture of CH_4 ($P_{CH_4} = 45$ Torr) and N_2 ($P_{N_2} = 225$ Torr). The total pressure of 270 Torr permitted the use of the $3f$ line locking technique in the entire range of the laser current modulation allowed by the CEU and corresponding to the wavelength peak-to-peak modulation of 0.013 to 0.44 cm^{-1}. This feature is important for comparing the QEPAS sensor performance at different gas pressures. The CEU electronics also includes the wall plug power supply, laser driver, and the diode laser in a $100 \times 250 \times 250$ mm^3 case with a keypad and LCD indicator. The CEU was equipped with a RS232 port for a digital computer interface. The digital output of CEU reported $2f$ components (in-phase and quadrature) of the QTF signal, $3f$ component of the PD signal, optical power, laser current, and periodically measured parameters of the QTF: its quality factor Q, resonant frequency f_0, and dynamic equivalent resistance R. The serial port also allowed remote control of the sensor operation, in particular setting such parameters as the laser current and modulation index by a LabView program.

The μR design used in this work was different from the previously reported versions consisting of two tubing pieces. Instead, the μR was formed by ∅0.35 mm holes drilled in two aluminum blocks. One of the aluminum blocks had ledges for confinement of the laser-generated sound wave between the prongs of the QTF (Fig. 1). It was determined that while these ledges increased the photoacoustic (PA) signal $\sim 30\%$, the surfaces of the aluminum blocks positioned close to the QTF planes reduced its Q factor ~ 2 times. Therefore, future ADM upgrades will use the tubing based μR design.

The QEPAS measurements were performed using two certified CH_4/N_2 gas mixtures, one with 101 ppmv CH_4 and another with 9.9 ppmv CH_4. All the experiments were performed in a gas flow varying from 100 to 500 sccm. No acoustic flow noise was detected. We also recorded methane spectra in ambient air pumped through the ADM gas cell.

The laser optical frequency as a function of its current, and the modulation amplitude, $\Delta\nu$ in terms of cm^{-1} as a function

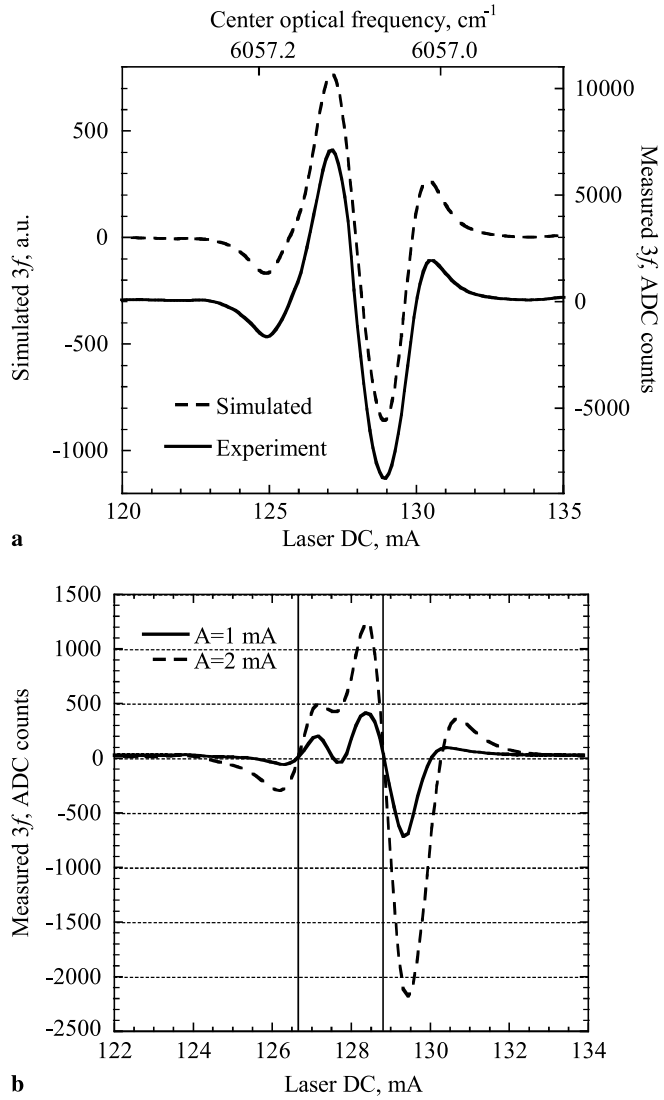

FIGURE 2 An example (**a**) showing the experimentally acquired $3f$ WM methane spectrum from the reference cell (*solid line*; 4 mA current modulation amplitude) and the corresponding numerically simulated spectrum (*dashed line*; 0.06 cm^{-1} modulation amplitude). Two zero crossings in the $3f$ WM spectra independent of the modulation amplitude (**b**)

of the current modulation amplitude, were calibrated using the $3f$ spectra from the reference cell acquired while scanning the laser current. For that purpose the $3f$ absorption spectra for different $\Delta\nu$ were simulated using parameters of CH_4 absorption lines from the HITRAN 2004 database, assuming Voigt line envelopes. An example of the simulated spectrum vs. the experimentally acquired data is shown in Fig. 2a. The spectral distance between certain zero crossing points was almost independent of the modulation amplitude (Fig. 2b) and used to calibrate the slow diode laser frequency tuning; the corresponding coefficient was found to be -3.24×10^{-2} cm^{-1}/mA. To determine the relation between the current modulation amplitude and the wavelength modulation amplitude, the theoretical spectral distance between the highest positive and negative peaks in the $3f$ spectra were compared to the observed distance for different current modulations (Fig. 3). Such a comparison yielded a ratio of 6.67×10^{-3} cm^{-1}/mA. Thus, the laser frequency is ~ 2 times

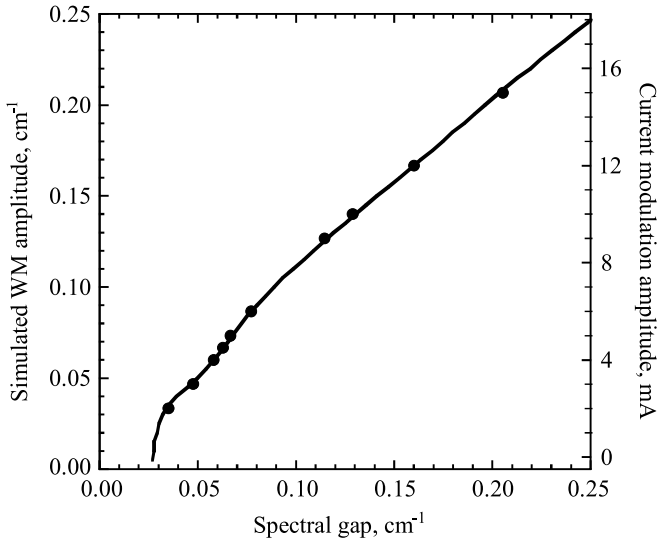

FIGURE 3 Amplitude of the diode laser current modulation as a function of the experimentally observed spectral gap between the highest positive and negative peaks in the $3f$ WM spectra from the reference cell (*circles*). WM modulation amplitude as a function of the same numerically simulated spectral gap (*line*)

more sensitive to fast (17 kHz) changes of the injection current than to its slow variations.

3 Performance optimization and sensitivity: CH_4 in dry N_2

A group of partially merged CH_4 absorption lines at 6057.1 cm^{-1} was selected for CH_4 monitoring purposes. Two examples of the QEPAS spectra acquired with different calibrated gas mixtures and at two different pressures are shown in Fig. 4. The quadrature component of the detected electrical signal is independent of the PA excitation and therefore allows evaluating the sensor noise. Based on the data from Fig. 4b, the rms noise in a $\Delta f = 0.0625$ Hz band is $N_{\text{exp}} = 0.482\,\mu$V. The thermal noise N of the QTF in each of the two quadrature components can be calculated using the equation ([1] and references therein)

$$N_{\text{th}} = \frac{1}{\sqrt{2}} R_{\text{FB}} \sqrt{\frac{4k_{\text{B}}T}{R}} \sqrt{\Delta f}\,. \tag{1}$$

With a transimpedance feedback resistor $R_{\text{FB}} = 10\,\text{M}\Omega$, $T = 297$ K, and a measured dynamic resistance of the QTF at 951 Torr nitrogen pressure $R = 220.7\,\text{k}\Omega$, (1) yields $N_{\text{th}} = 0.481\,\mu$V. Thus, the sensor noise is at the fundamental thermal noise limit.

Signal S detected by means of QEPAS can be expressed as

$$S(P) = KI[\text{CH}_4]Q(P)\beta(P)\varepsilon(P)\,, \tag{2}$$

where K, I and $[\text{CH}_4]$ are respectively the sensor constant, laser power, and CH_4 concentration and do not depend on the total gas pressure P. Other coefficients are pressure dependent: the QTF Q factor, the peak of $2f$ WM absorption spectrum β, and the conversion efficiency of the absorbed optical power into the sound ε (more accurately, its Fourier component at f_0 frequency). For simplicity we shall assume

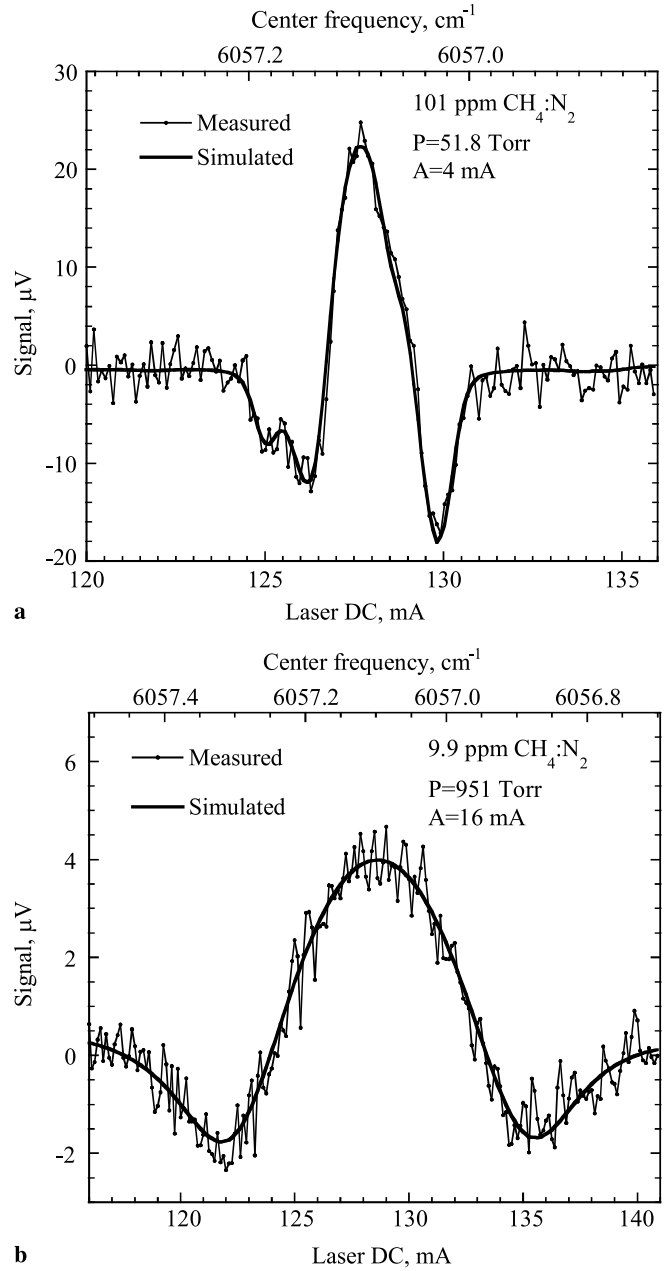

FIGURE 4 QEPAS spectra and corresponding HITRAN 2004-based line shape simulations. *Vertical axis* shows the voltage measured at the transimpedance pre-amplifier output with a 10 MΩ feedback resistor, additionally amplified 30 times. (**a**) 101 ppmv CH_4 in N_2 mixture, 52 Torr pressure, $A = 4$ mA diode laser current modulation amplitude, lock-in amplifier time constant $\tau = 1$ s with 12 dB/oct filter slope ($\Delta f = 0.25$ Hz); (**b**) 9.9 ppmv CH_4 in N_2 mixture, 951 Torr pressure, $A = 16$ mA, $\tau = 3$ s with 18 dB/oct filter slope ($\Delta f = 0.0625$ Hz)

$K \equiv 1$ and omit this constant scaling figure in the equations below.

It was found that $Q(P)$ is well described by the empirical equation

$$Q(P) = 35290P^{-0.29}\,, \tag{3}$$

where P is in Torr. The $\beta(P)$ dependence together with the corresponding optimum laser WM amplitude, $A(P)$, were calculated based on the laser spectral calibration described

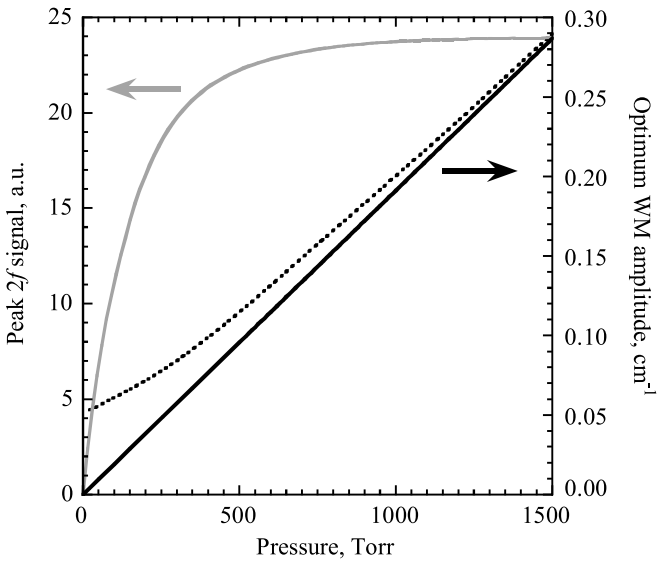

FIGURE 5 Optimum WM amplitude $A(P)$ (*dotted curve*) and the corresponding CH_4 (6057.1 cm^{-1}) $2f$ WM peak value $\beta(P)$ as a function of the carrier gas pressure (*solid gray curve*); CH_4 concentration is assumed constant. *Solid straight black line*: asymptotically optimum WM amplitude at high gas pressure

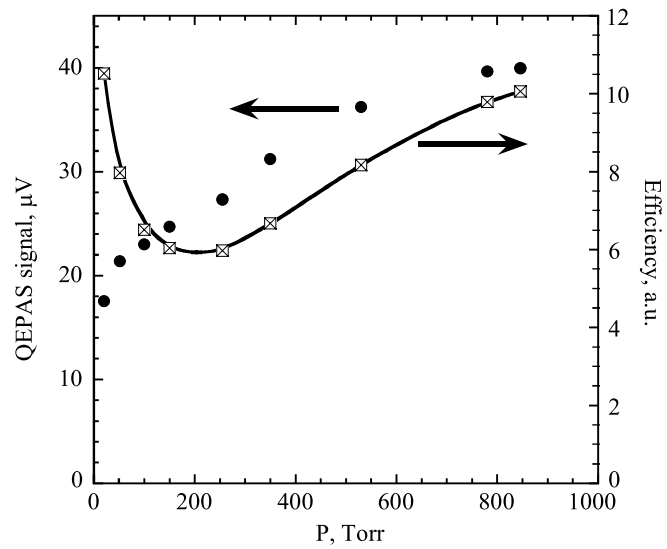

FIGURE 6 Measured QEPAS signal (*circles*) and the derived efficiency of the optical radiation-to-sound conversion $\varepsilon(P)$ (*squares with a smoothing curve*) for CH_4 in dry N_2

in the previous section and HITRAN data. In these simulations the self-broadening coefficient was neglected because of the low CH_4 concentration. The numerically simulated $2f$ WM line shapes corresponding to particular experimental conditions are shown in Fig. 4. The perfect coincidence of the experimental data and theoretical predictions proves the accuracy of the HITRAN pressure broadening coefficients for these lines and validity of our approach. Figure 5 presents optimum $A(P)$ and the corresponding $\beta(P)$for the selected group of CH_4 lines at 6057.1 cm^{-1} in the 0–1500 Torr pressure range. Using (31) and (32) from [11] and numerical calculations, the modulation width resulting in the highest $2f$ signal for a Lorentzian-shaped absorption line can be found to be $A \approx 2.20$ HWHM. Hence, for these CH_4 lines with atmospheric pressure broadening coefficients of HWHM = 0.066 cm^{-1}/atm (HITRAN 2004) the asymptotically optimum modulation is $A = 1.911 \times 10^{-4}$ cm^{-1}/Torr, which is shown as a straight line in Fig. 5 plot.

With a knowledge of $\beta(P)$ and $A(P)$, $\varepsilon(P)$ can be calculated from (2) using the experimentally measured $S(P)$. The QEPAS signal measured for the 101 ppmv mixture at different pressures was used for calculating $\varepsilon(P)$. The WM amplitude was not always optimum, and the necessary correction was made when calculating $\varepsilon(P)$ .The results are shown in Fig. 6. The increase of $\varepsilon(P)$ from 200 Torr towards lower pressures is tentatively explained by the diffusion of the initially excited molecules to the μR tube wall with the subsequent V–T relaxation on the wall. Indeed, Wakeham et al. [12] measured the diffusion coefficient in the CH_4/N_2 mixture at $T = 297$ K and atmospheric pressure to be $D_{12} = 0.21$ cm^2/s. The mean diffusion path traveled by an excited CH_4 molecule from the initial position on the μR axis (2D diffusion) in t [s] is

$$\sqrt{\langle r^2 \rangle} = \sqrt{4 D_{12} \frac{P_{\mathrm{atm}}}{P} t} \,. \tag{4}$$

Substituting 100 Torr for P and $1/f_0 = 30.5$ μs for t, we obtain $\sqrt{\langle r^2 \rangle} = 140$ μm, which is comparable with the μR radius of 175 μm. Thus, a significant fraction of excited molecules will reach the μR wall in one modulation period, which can impact the effective molecular relaxation rate.

The increase of $\varepsilon(P)$ towards higher pressures is due to the increased rate of molecular collisions and hence a faster V–T relaxation. If diffusion is neglected, $\varepsilon(P)$ according to [9, 13, 14] can be expressed as

$$\varepsilon(P) = \frac{1}{\sqrt{1 + \frac{[2\pi f(P_0 \tau_0)]^2}{P^2}}} \,. \tag{5}$$

This equation can be rewritten as

$$\left[\frac{1}{\varepsilon(P)}\right]^2 = 1 + \frac{[2\pi f(P_0 \tau_0)]^2}{P^2} \,. \tag{6}$$

It follows from (6) that a simple linear fit of $[1/\varepsilon(P)]^2$ as a function of $1/P^2$ at higher pressures will yield the relaxation time constant, $P_0 \tau_0$. To achieve a higher accuracy of this constant, we performed an additional set of QEPAS measurements in the pressure range 500–900 Torr. Their results, along with a linear fit in $1/P^2$–$[K/\varepsilon(P)]^2$ coordinates, are shown in Fig. 7. According to (6), the $[2\pi f(P_0 \tau_0)]^2$ value is equal to the ratio of this fit slope to the fit offset. We calculated $P_0 \tau_0 = 2.9 \pm 0.2$ ms Torr based on the data presented. This value is close to the relaxation rate measured for HCN in N_2 [9], 2.2 ± 0.4 ms Torr.

Now that all the three functions $Q(P)$, $\beta(P)$, and $\varepsilon(P)$ are known for $P > 400$ Torr, (2) can be used to evaluate the sensor performance in terms of the observed signal $S(P)$ and SNR $\sim \frac{S(P)}{\sqrt{Q(P)}}$ at a given CH_4 concentration. The corresponding curves are presented in Fig. 8. They predict that the strongest signal is obtained at 1030 Torr, while the highest SNR would be reached at 1505 Torr. It should be noticed that both functions are slow, and vary less than 10% in the 760–2000 Torr gas pressure range.

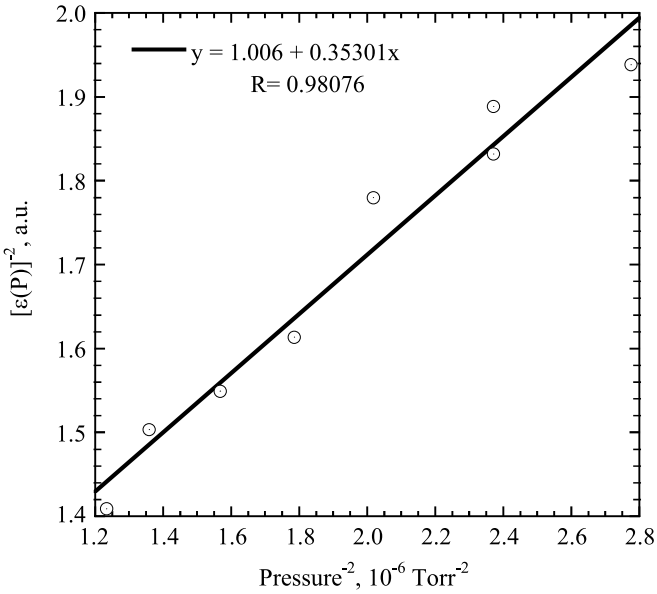

FIGURE 7 Experimental results (*circles*) and linear fit for determining the V–T relaxation rate of CH_4 $2\nu_1$ state in dry N_2

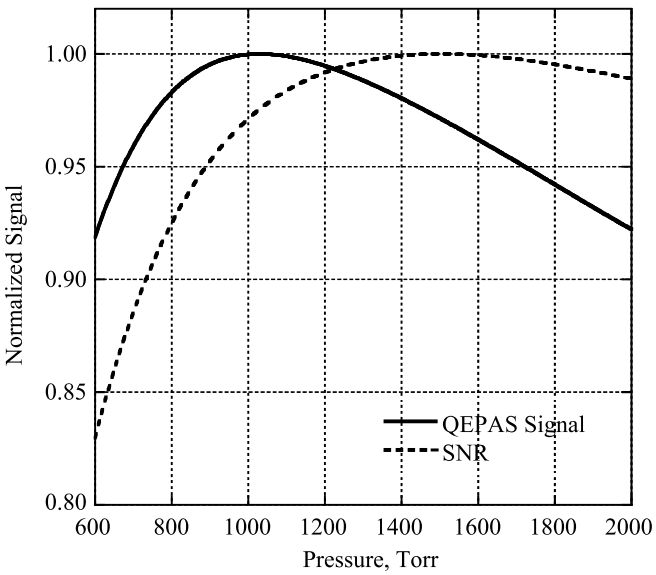

FIGURE 8 Plot of conversion efficiency extrapolated to higher pressures to show the optimum operating pressure for the QEPAS sensor to detect CH_4 in dry N_2. The predicted QEPAS sensor performance is based upon the developed relaxation model. The signal-to-noise ratio (SNR) is also plotted

The absolute sensitivity of the QEPAS sensor to CH_4 in dry N_2 was evaluated using the scan depicted in Fig. 4b. The noise equivalent CH_4 concentration was found to be $[CH_4]_{min} = 66$ ppmv mW/Hz$^{1/2}$, and the normalized noise equivalent absorption coefficient, NNEA $= 2.9 \times 10^{-8}$ cm^{-1} W/Hz$^{1/2}$.

4 Performance optimization and sensitivity: CH_4 in wet N_2

The observed QEPAS signal generated at a certain CH_4 concentration in the gas mixture was much stronger in the presence of H_2O vapor. This is illustrated by Fig. 9, depicting the detected QEPAS signal normalized to the changing

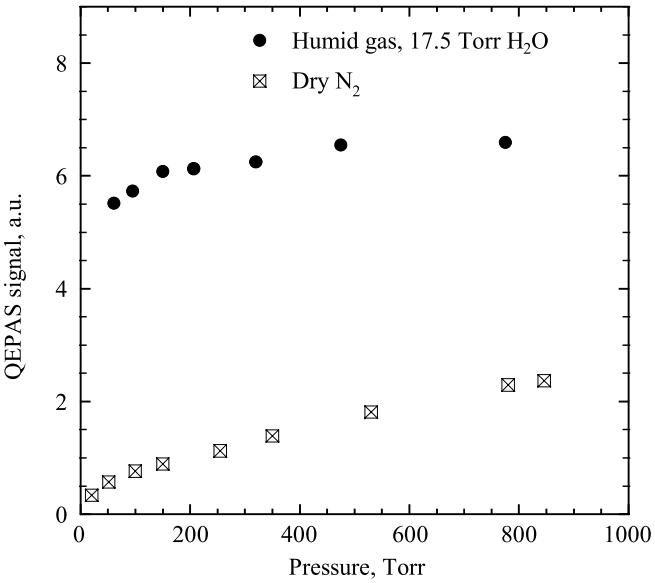

FIGURE 9 Observed QEPAS signal for trace CH_4 in dry N_2 (*squares*) and N_2 with saturated H_2O vapor at +24 °C (*circles*) as a function of the total gas pressure. All data normalized to CH_4 concentration and the QTF Q factor

Q factor (lower in a humid gas) and to the methane concentration in the gas. Analysis of this data reveals that such an increase in the QEPAS signal cannot be explained solely by the increased V–T relaxation rate of the initially excited CH_4 vibration. Indeed, for dry N_2 at 600 Torr $\varepsilon(600\,\text{Torr}) = 0.71$ according to (5), and hence even an instantaneous relaxation ($P_0\tau_0 = 0$) in the frames of the model outlined in the previous section would result only in $\sim 30\%$ increase of the QEPAS signal. This leads us to the conclusion that the relaxation constant of 2.9 ms Torr derived in the previous section describes only the initial fast step of the excited CH_4 molecule relaxation in dry N_2, followed by slower V–T energy transfer from lower vibrational levels. This is likely to be a transition from the initially excited $2\nu_2$ state of P4 tetradecad to $3\nu_4$ state of the lower P3 octad [8]. Such a transition would release $\sim 1/3$ of the vibrational energy, approximately matching the ratio of signals observed between dry and wet gases at high pressures (Fig. 9).

To analyze the H_2O influence quantitatively, the QEPAS signal following the optical CH_4 excitation was studied at 150 Torr pressure and at varying low H_2O concentrations. We assume that the part of the initial vibrational excitation energy released via CH_4/N_2 collisions remains constant and results in unchanged S_1 portion of the signal, while the signal S_2 due to CH_4/H_2O collisions exhibit a dependence on H_2O partial pressure, P_H, according to (5):

$$S(P_H) = S_1 + S_2 = S_1 \left(1 + \frac{R-1}{\sqrt{1 + \frac{(2\pi f \tau_0^H P_0)^2}{P_H^2}}} \right) . \qquad (7)$$

Here $R = \frac{S(\infty)}{S(0)}$; we assume that the observed signal at the saturated H_2O pressure is equal to $S(\infty)$. From experimental results (Fig. 9) the value of $R = 6.8$ at 150 Torr total pressure. A constant $\tau_0^H P_0$ describes V–T relaxation rate due to

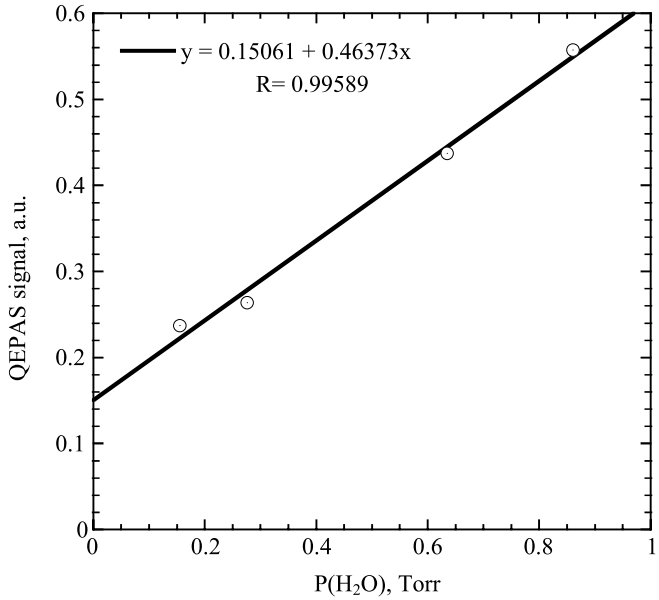

FIGURE 10 QEPAS signal (*circles*) as a function of H_2O concentration in a weakly humid CH_4/N_2 gas, together with a linear fit

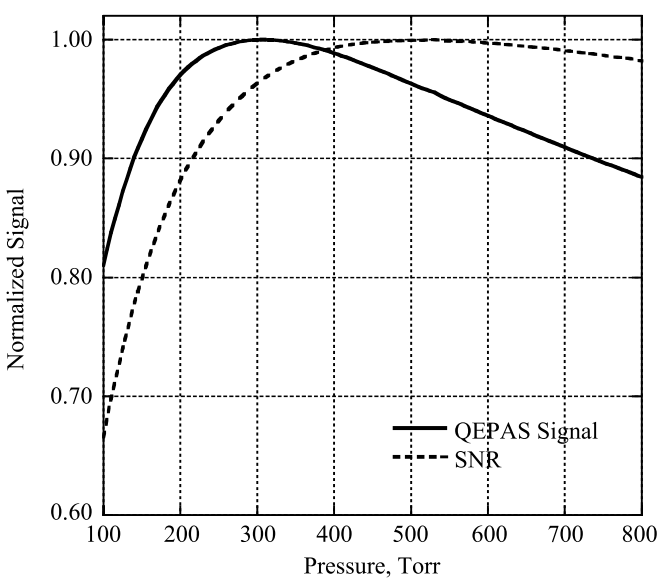

FIGURE 11 Predicted QEPAS sensor performance for detecting CH_4 in wet N_2 ($P_H > 2$ Torr) at different pressures based on the developed relaxation model

CH_4:H_2O collisions. If $\frac{(2\pi f \tau_0^H P_0)^2}{P_H^2} \gg 1$, a linear approximation can be used for S_2:

$$S(P_H) \approx S_1 \left[1 + (R-1) \frac{P_H}{2\pi f \tau_0^H P_0} \right]. \quad (8)$$

Such a linear fit of the experimental results is shown in Fig. 10. The fitting parameters yield $\tau_0^H P_0 = 9.2 \pm 0.5$ µs Torr. Using (5) we can now calculate that QEPAS signal would reach 95% of its instantaneous-relaxation value at 1.9 Torr partial H_2O pressure, and 90% at 1.3 Torr partial H_2O pressure. This corresponds to respectively 8.5% and 5.8% relative humidity at +24 °C. In gas samples with $P_H > 2$ Torr, the V–T relaxation of CH_4 can be considered instantaneous compared to $1/2\pi f$ time. In such a case $\varepsilon = 1$ in (2), and QEPAS sensor responsivity will be determined solely by the $\beta(P)Q(P)$ product. This function is evaluated using the previously calculated value of $\beta(P)$ (Fig. 6) and (3) for $Q(P)$, and plotted in Fig. 11. This plot also shows the SNR dependence on gas pressure determined by $\beta(P)\sqrt{Q(P)}$. The QEPAS signal peaks at 306 Torr, while the SNR has a smooth maximum at 500 Torr.

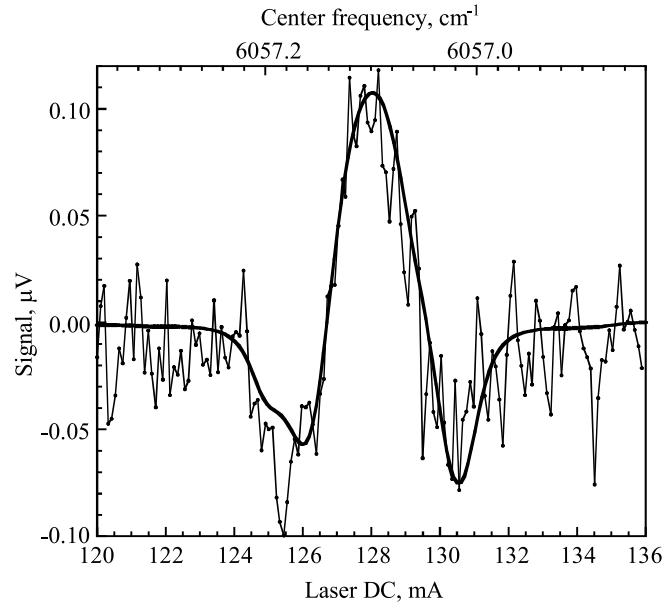

FIGURE 12 QEPAS spectrum (*circles*) of CH_4 near 6057.1 cm^{-1} in ambient air sample at 150 Torr and numerically simulated $2f$ WM line shape (*solid line*). The signal shown is the transimpedance pre-amplifier output rms voltage without additional amplification

A spectral scan of an ambient air sample at 150 Torr that includes the CH_4 absorption peak at 6057.1 cm^{-1} (Fig. 12) is in agreement with this conclusion. Using the CH_4 in dry N_2 calibration and a scaling coefficient from the high-humidity measurements (Fig. 9) to account for the H_2O presence, the CH_4 concentration in an ambient air sample was calculated to be 2.0 ppmv, which is close to the average 1.75 ppmv ambient atmospheric concentration. Atmospheric CH_4 concentrations exceeding 2 ppmv are not unusual, see for example [15]. The evaluated detection sensitivity for wet (> 2 Torr partial H_2O pressure) gas samples is $[CH_4]_{min} = 24$ ppmv mW/Hz$^{1/2}$, and the NNEA $= 1.0 \times 10^{-8}$ cm^{-1} W/Hz$^{1/2}$.

5 Conclusions

Sensitivity has been previously reported for conventional PAS-based detection of CH_4 [8] with an 8 mW laser accessing the same 6057.1 cm^{-1} absorption peak. A noise-equivalent concentration of 0.06 ppmv CH_4 was achieved with a 970 Hz modulation frequency, a 10 s lock-in amplifier time constant, and a 12 dB/oct low-pass filtering (details were provided by Dr. S. Schilt of IR Microsystems). Measurements [8] were performed at atmospheric pressure, and the results were not sensitive to changes in H_2O concentration in the CH_4 in N_2 mixture. This is obviously due to the lower modulation frequency (970 Hz) as compared to the 32.8 kHz of our QEPAS-based measurements. This result converts to 3 ppmv mW/Hz$^{1/2}$, or an ∼ 8 times better

sensitivity than what we observed with our QEPAS sensor for wet gas samples. We believe that the difference in detection sensitivity is primarily explained by an ~ 34 times difference in the modulation frequency. However, the QEPAS approach delivers a more compact and lightweight sensor and thus is advantageous for applications that do not require ultimate detection sensitivity. For example, the QEPAS sensor can detect noise-equivalent CH_4 levels of 0.2 ppmv with a 1 min data acquisition time (i.e., $\sim 3\times$ time constant). We expect ~ 2 times improvement with further optimization of the QEPAS ADM, especially in the microresonator design.

ACKNOWLEDGEMENTS This work was performed under the auspices of the U.S. Department of Energy contract # DE-AC09-96SR18500. Additional support of the research performed by the Rice Laser Science group was provided by the National Aeronautics and Space Administration via awards from the Jet Propulsion Laboratory, Pasadena, CA and Johnson Space Center, Houston, TX, the National Science Foundation via a subaward from the Princeton University MIRTHE ERC and the Robert Welch Foundation.

The authors wish to thank Dr. S. Schilt of IR Microsystems, Inc, Lausanne, Switzerland for helpful discussions of methane vibrational relaxation dynamics.

REFERENCES

1 A.A. Kosterev, F.K. Tittel, D.V. Serebryakov, A.L. Malinovsky, I.V. Morozov, Rev. Sci. Instrum. **76**, 043 105 (2005)
2 A.A. Kosterev, Y.A. Bakhirkin, R.F. Curl, F.K. Tittel, Opt. Lett. **27**, 1902 (2002)
3 M.D. Wojcik, M.C. Phillips, B.D. Cannon, M.S. Taubman, Appl. Phys. B **85**, 307 (2006)
4 R. Lewicki, G. Wysocki, A.A. Kosterev, F.K. Tittel, Opt. Express **15**, 7357 (2007)
5 A.A. Kosterev, Y.A. Bakhirkin, F.K. Tittel, S. Blaser, Y. Bonetti, L. Hvozdara, Appl. Phys. B **78**, 673 (2004)
6 G. Wysocki, A.A. Kosterev, F.K. Tittel, Appl. Phys. B **85**, 301 (2006)
7 R. Lewicki, G. Wysocki, A.A. Kosterev, F.K. Tittel, Appl. Phys. B **87**, 157 (2007)
8 S. Schilt, J.-P. Besson, L. Thévenaz, Appl. Phys. B **82**, 319 (2006)
9 A.A. Kosterev, T.S. Moseley, F.K. Tittel, Appl. Phys. B **85**, 295 (2006)
10 S. Schilt, L. Thévenaz, P. Robert, Appl. Opt. **42**, 6728 (2003)
11 C. Forbes Dewey Jr., *Optoacoustic Spectroscopy and Detection*, ed. by Y.-H. Pao (Academic, New York, San Francisco, London, 1977), Chapt. 3
12 W.A. Wakeham, D.H. Slater, J. Phys. B **6**, 886 (1973)
13 G. Gorelik, Dokl. Akad. Nauk SSSR **54**, 779 (1946) (in Russian)
14 T.L. Cottrell, J.C. McCoubrey, *Molecular Energy Transfer in Gases* (Butterworths, London, 1961)
15 D. Romanini, M. Chenevier, S. Kassi, M. Schmidt, C. Valant, M. Ramonet, J. Lopez, H.-J. Jost, Appl. Phys. B **83**, 659 (2006)